Journal of Biomedical Optics

BiomedicalOptics.SPIEDigitalLibrary.org

Vibrational mapping of sinonasal lesions by Fourier transform infrared imaging spectroscopy

Elisabetta Giorgini
Simona Sabbatini
Carla Conti
Corrado Rubini
Romina Rocchetti
Massimo Re
Lisa Vaccari
Elisa Mitri
Vito Librando

SPIE.

Vibrational mapping of sinonasal lesions by Fourier transform infrared imaging spectroscopy

Elisabetta Giorgini,[a,*] Simona Sabbatini,[b] Carla Conti,[b] Corrado Rubini,[c] Romina Rocchetti,[a,c] Massimo Re,[d] Lisa Vaccari,[e] Elisa Mitri,[e] and Vito Librando[f]

[a]Università Politecnica delle Marche, Dipartimento di Scienze della Vita e dell'Ambiente, Via Brecce Bianche, 60131 Ancona, Italy
[b]Università Politecnica delle Marche, Dipartimento di Scienze e Ingegneria della Materia, dell'Ambiente ed Urbanistica, Via Brecce Bianche, 60131 Ancona, Italy
[c]Università Politecnica delle Marche, Dipartimento di Scienze Biomediche e Sanità Pubblica, Via Conca, 71, 60126 Torrette (Ancona), Italy
[d]Università Politecnica delle Marche, Dipartimento di Malattie Immuno-Allergiche e Respiratorie, Via Conca, 71, 60126 Torrette (Ancona), Italy
[e]Elettra—Sincrotrone Trieste, S.S. 14, Km 163.5, 34012 Basovizza (Trieste), Italy
[f]Università degli Studi di Catania, Dipartimento di Scienze Chimiche, Via Andrea Doria, 6, 580138 Catania, Italy

Abstract. Fourier transform infrared imaging (FTIRI) is a powerful tool for analyzing biochemical changes in tumoral tissues. The head and neck region is characterized by a great variety of lesions, with different degrees of malignancy, which are often difficult to diagnose. Schneiderian papillomas are sinonasal benign neoplasms arising from the Schneiderian mucosa; they can evolve into malignant tumoral lesions (squamous cell carcinoma). In addition, they can sometimes be confused with the more common inflammatory polyps. Therefore, an early and definitive diagnosis of this pathology is mandatory. Progressing in our research on the study of oral cavity lesions, 15 sections consisting of inflammatory sinonasal polyps, benign Schneiderian papillomas, and sinonasal undifferentiated carcinomas were analyzed using FTIRI. To allow a rigorous description of these pathologies and to gain objective diagnosis, the epithelial layer and the adjacent connective tissue of each section were separately investigated by following a multivariate analysis approach. According to the nature of the lesion, interesting modifications were detected in the average spectra of the different tissue components, above all in the lipid and protein patterns. Specific band-area ratios acting as spectral markers of the different pathologies were also highlighted. [DOI: 10.1117/1.JBO.20.12.125003]

Keywords: Fourier transform infrared imaging; sinonasal lesions; Schneiderian papilloma; sinonasal undifferentiated carcinoma; multivariate analysis.

Paper 150444RR received Jul. 8, 2015; accepted for publication Nov. 11, 2015; published online Dec. 16, 2015.

1 Introduction

The head and neck region is a complex anatomical area with a great variety of lesions, from inflammatory pathologies to benign and malignant neoplasia. Many of these lesions are infrequently observed. Therefore, pathologists do not have the opportunity of becoming familiar with them.[1] For this reason, a correct diagnosis should not be merely restricted to morphological details investigated through histopathological, immunohistochemical, and radiological techniques.[2]

Fourier transform infrared imaging (FTIRI), together with conventional biomedical assays,[3] is an objective and well-established analytical technique for the unambiguous diagnosis of cancerous and precancerous lesions. By acquiring IR images of biological samples (fluids, cells, and tissues), it is possible to obtain reliable and reproducible information on their biochemical composition. In addition, it is possible to monitor with high accuracy the compositional and structural changes caused by tumoral pathologies by analyzing functional groups, bonding types, and molecular conformations of the most relevant biomolecules.[4–7] Many contributions describe the use of infrared spectroscopy to detect cancerous lesions in a very early stage of the pathology, even before any morphological evidence can be detected.[8,9]

In the past decade, we have been studying from a vibrational point of view various epithelial pathologies that may affect the oral compartment.[10–13] In most cases, the IR imaging approach played a key role in detecting early stages of inflammatory, benign, and malignant diseases, helping to gain a deeper understanding of the etiologic nature of different pathologies.

Sinonasal inflammatory polyps (SNPs) are common nonneoplastic lesions of the sinonasal mucosa. They frequently originate from allergic rhinitis and may cause the onset of some biochemical alterations in the epithelial layer, not always easily detectable by routine immunohistochemical assays. They show an intact respiratory epithelium and may present polymorphic stromal cells, which can be confused with malignant ones. The presence of some inflammatory cell aggregations is demonstrated by patches of stromal nonedematous collagen.[2] Schneiderian papillomas (BSPs) are sinonasal benign neoplasms arising from the Schneiderian mucosa. They are classified into three different varieties: fungiform, oncocytic, and inverted. The latter, considered the most common type, is characterized by a transitional epithelium with squamous, transitional, and columnar cells.[1,2] These papillomas have the tendency to recur, destroying neighboring tissues, and to progress into more aggressive squamous cell carcinomas. For these reasons, they are primarily treated with a rather invasive surgical resection; when necessary, radiation therapy follows

*Address all correspondence to: Elisabetta Giorgini, E-mail: e.giorgini@univpm.it

1083-3668/2015/$25.00

and a close follow-up of the patient is recommended. Sinonasal undifferentiated carcinomas (SNUCs) are high-grade malignant epithelial tumors, arising both *ex novo* and from Schneiderian papillomas. They are characterized by hypercellular proliferation and by the presence of squamous foci with high amounts of keratin.[2]

The association of Schneiderian papillomas with malignant carcinomas and their tendency to be confused with more common benign lesions, such as SNPs, make it necessary to explore new methods for their reliable diagnosis.[14] To improve the knowledge in this field, we performed FTIRI on different inflammatory and neoplastic sinonasal lesions, such as SNPs, BSPs, and SNUCs. Visible and infrared images of each section were acquired and the biomolecular features of the epithelial and connective components were evaluated, pinpointing specific spectral markers of each pathology.

2 Experimental Section

2.1 *Sample Preparation*

Fifteen tissue samples, collected from consenting patients by surgical resection of the sinonasal region, were analyzed: n. 6 SNP, n. 4 BSP, and n. 5 SNUC. To participate in this research, also approved by the local Ethical Committee, all the patients signed an informed consent. They received surgical treatment for therapeutic purposes without any previous pharmaceutical treatment. A preliminary classification of all the samples was carried out, according to World Health Organization guidelines, by comparing clinical, radiological, and histological outcomes.

For each sample, three groups of twin adjacent sections (5 to 7 μm thick) were cryosectioned: the first sections were deposited onto glass slides for histological examination [hematoxylin and eosin (H&E) staining], and the latter ones were deposited without any fixation process onto CaF_2 optical windows (1-mm thick) and air-dried for 30 min for infrared analysis.[11] A total of 45 sections were analyzed (18 sections for SNPs, 12 for BSPs, and 15 for SNUCs).

2.2 *FTIR Measurements and Data Analysis*

FTIR measurements were carried out at the IR beamline SISSI, ELETTRA—Sincrotrone Trieste, using a Bruker VERTEX 70 interferometer coupled with a Hyperion 3000 Vis–IR microscope and equipped with a liquid nitrogen–cooled bidimensional FPA detector (detector area size 64×64 pixels; Bruker Optics GmbH, Germany). Using a 15× condenser/objective, the visible image of each section was achieved, whereas IR maps of specific areas ($\approx 160 \times 490$ μm^2 with a pixel resolution of about 2.56 μm), selected according to the pathologist's suggestions, were acquired in transmission mode (12,288 spectra, 256 scans, spectral resolution 4 cm^{-1}). Background spectra were acquired on a clean portion of the CaF_2 windows. Raw spectra were pretreated by simply applying the atmospheric compensation routine of OPUS 7.1 for atmospheric CO_2 and water vapor correction.

To evaluate the spatial distribution of the principal biocomponents (lipids, proteins, and nucleic acids), false color images were calculated by integrating IR maps under the following spectral regions: CH stretching region (3050 to 2800 cm^{-1}), amide I and II bands (1720 to 1480 cm^{-1}), and phosphates and carbohydrates zone (1350 to 900 cm^{-1}). For this purpose, R package HyperSpec was used.[15] Before integration, spectra were vector normalized for avoiding artifacts induced by local thickness variations.

To discriminate the spectra corresponding to epithelial and connective components, for each IR map, unsupervised hierarchical cluster analysis (UHCA) was applied to preprocessed spectra in the 1800 to 900 cm^{-1} spectral range upon two-points baseline linear fit and vector normalization. The Euclidean distance and Ward's algorithm were used in order to group spectra according to their similarity. The obtained clusters were localized on the sections using a topographical method, and their position was cross-validated by the histological examination of the corresponding H&E sections. The spectra of all epithelia-belonging pixels were resubmitted to principal component analysis (PCA). The same procedure was followed for the spectra of connective clusters.

For each section, average spectra of the epithelium layer and connective tissue were analyzed in absorbance and second derivative (DII, nine-points smoothing) mode. In addition, to calculate the areas of the component bands, a peak-fitting (Gaussian algorithm) procedure was applied to average absorbance spectra in the following spectral ranges: 3050 to 2800 cm^{-1} (lipids), 1800 to 1480 cm^{-1} (proteins), and 1480 to 920 cm^{-1} (carbohydrates and phosphates). Both the number and center of the subcomponent bands were fixed according to DII results. Mean values of area and wavelength were evaluated for each component band and assigned according to previous studies.[11]

The whole methodological process of the study is sketched in Fig. 1.

For data handling, the following software packages were used: OPUS 7.1 (Bruker Optics GmbH, Germany), HyperSpec, Pirouette 4.5 (Infometrix Inc.), and GRAMS/AI 9.1 (Galactic Industries, Inc., Salem, New Hampshire).

2.3 *Statistical Analysis*

Band-area ratios were presented as mean $\pm$ SD. Significant differences between experimental groups were determined by means of a factorial analysis of variance (one-way ANOVA), followed by Tukey's multiple comparisons test, using the statistical software package Prism5 (Graphpad Software, Inc.). Significance was accepted at $P < 0.05$.

3 Results and Discussion

All the samples were first submitted to histological examination to detect meaningful structural differences, both in the epithelial layers and in the connective tissues. As an example, in Fig. 2, three sections representative of SNPs, BSPs, and SNUCs were reported. In the section of the SNP, a thin cellular layer of respiratory epithelium (rE) was detected surrounding the whole sample; beneath the epithelial membrane, two zones of loose connective tissue (Co), consisting of amorphous ground substance with loose extracellular fibers and different types of connective tissue cells, were highlighted, together with a large area of inflammatory infiltrate (iI), characterized by an inflammatory granulation tissue. In the section of the BSP, a trE internally growing into the stroma by forming some crypts, was found in the outer limit of the sample; the inner part was composed of loose connective tissue (Co). In the SNUC, two large areas of tumoral epithelium (tE) spaced apart by a small zone of residual Co, not yet infiltrated, were detected.

For each section, according to the pathologist's suggestions, IR chemical images were acquired on specific areas, containing

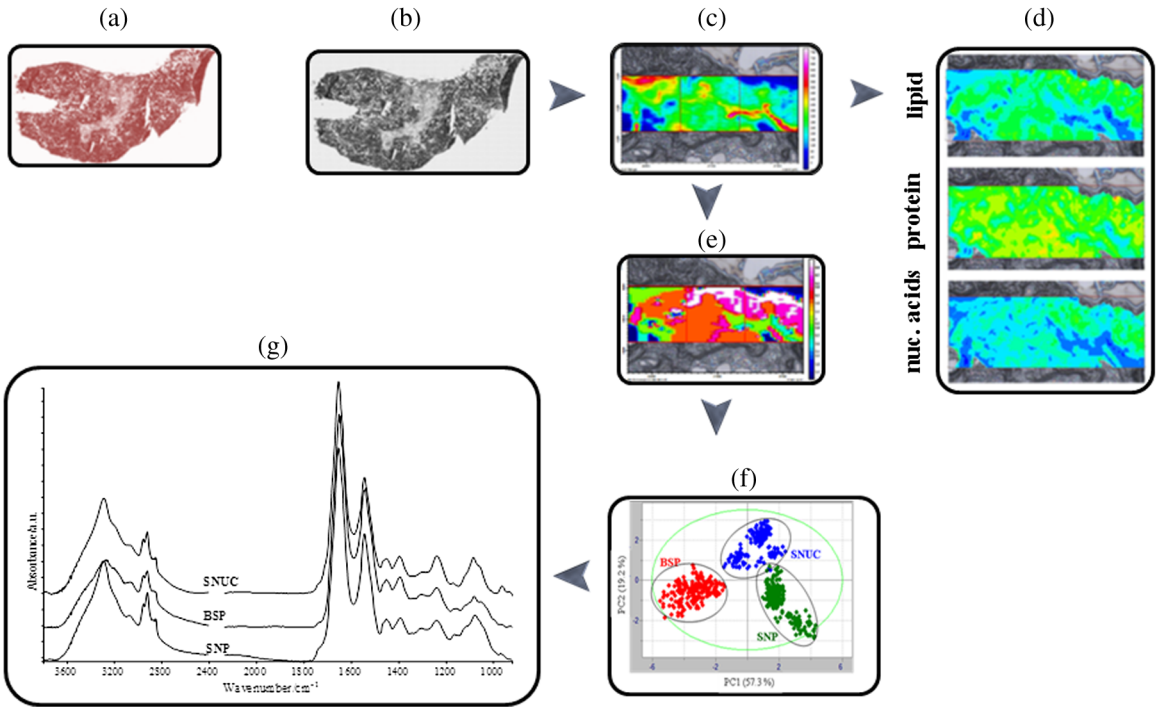

Fig. 1 Methodological process. Each sample was submitted both to (a) histological and (b) FTIR Imaging analysis. On specific areas, the (c) IR maps were acquired, on which (d) false color images, corresponding to the distribution of lipids, proteins, and nucleic acids, were calculated. IR data were then submitted to multivariate analysis, (e) UHCA and (f) PCA, from which (g) absorbance average spectra were achieved both for epithelia and connectives.

both the epithelial layer and the neighboring connective tissue. In Fig. 3(a), the microphotographs of three acquired areas, representative of SNP, BSP, and SNUC sections, were reported. To localize the distribution of lipids, proteins, and nucleic acids inside the investigated zones, false color images of each section were calculated by integrating under the following spectral regions: 3050 to 2800 cm^{-1} [lipids, Fig. 3(b)], 1720 to 1480 cm^{-1} [proteins, Fig. 3(c)], and 1350 to 900 cm^{-1} [nucleic acids, Fig. 3(d)]. By analyzing false color images, a relatively lower content of lipids and nucleic acids with respect to proteins was evident for all the experimental groups, as expected due to the nature of these tissues. Moreover, for all the sections, a clear colocalization of lipids and proteins was found. The same trend was less evident for the nucleic acids.

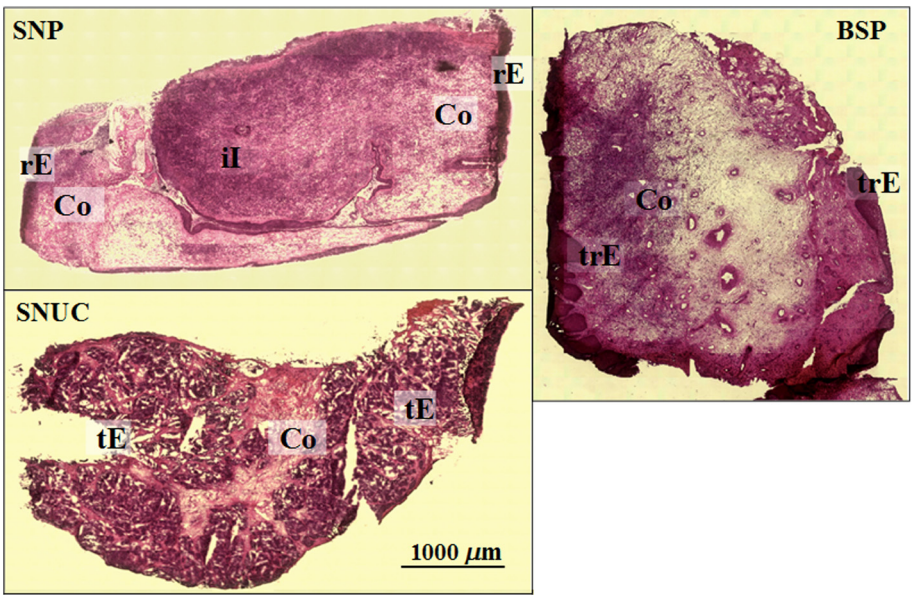

Fig. 2 Visible images of the following H&E tissue sections: inflammatory sinonasal polyp (SNP), benign inverted Schneiderian papilloma (BSP), and squamous undifferentiated carcinoma (SNUC). Various tissue components were identified: rE, respiratory epithelium; trE, transitional epithelium; tE, tumoral epithelium; Co, connective tissue; and iI, inflammatory infiltrate.

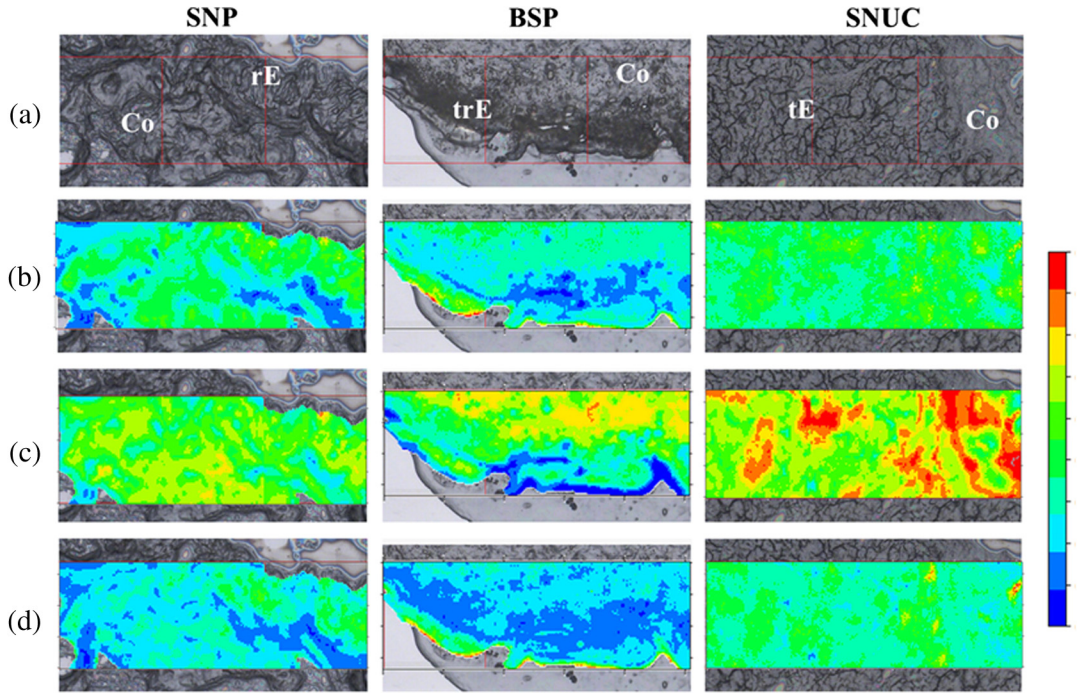

Fig. 3 (a) Visible images of SNP, BSP, and SNUC tissue sections. The areas acquired by FTIRI spectroscopy (red squares) included various tissue components: rE, respiratory epithelium; trE, transitional epithelium; tE, tumoral epithelium; and Co, connective tissue. For each section, false color images corresponding to the distribution of lipids, proteins, and nucleic acids were reported, obtained by integrating the IR maps under the following spectral regions: (b) 3050 to 2800 cm^{-1}, lipids (color scale 0.000 to 0.010 a.u.); (c) 1800 to 1480 cm^{-1}, proteins (color scale 0.000 to 0.0450 a.u.); and (d) 1350 to 920 cm^{-1}, nucleic acids (color scale 0.000 to 0.012 a.u.). Each acquired area corresponded to 492×164 μm^2.

By means of UHCA on the raw spectra of each section, the ones belonging to the clusters of the epithelial and connective components were isolated, then independently resubmitted to PCA. As shown in the PCA score plot of epithelia [Fig. 4(a)], three well-segregated clusters were detected in the PC1–PC2 space, where the first and second principal components account for the total spectral variability in the amount of 57.3% and 19.2%, respectively. This result confirmed the histological suggestion of the occurrence of different epithelia in SNP, BSP, and SNUC lesions. In the PC1 (69.9%) versus PC2 (10.1%) score plot of connectives [Fig. 4(b)], only the cluster corresponding to the tumoral connective was fully segregated, in agreement with the presence, in the neighboring of tE, of an altered connective tissue produced by the tumor itself.[12,16] The other two clusters corresponding to SNP and BSP specimens were partially overlapped, pinpointing that connective inflammation was a common feature of both SNPs and BSPs, and unveiling one of the reasons it is hard to diagnose these two pathologies.

3.1 *Vibrational Analysis of Epithelia*

To highlight specific spectral markers of each pathology, the average spectra of the different epithelia found in SNP, BSP, and SNUC lesions (Fig. 5) were analyzed using the peak-fitting procedure in the following spectral regions: 3050 to 2800 cm^{-1} (alkyl stretching modes), 1800 to 1480 cm^{-1} (amide I and II), and 1350 to 920 cm^{-1} (nucleic acid; data not shown).

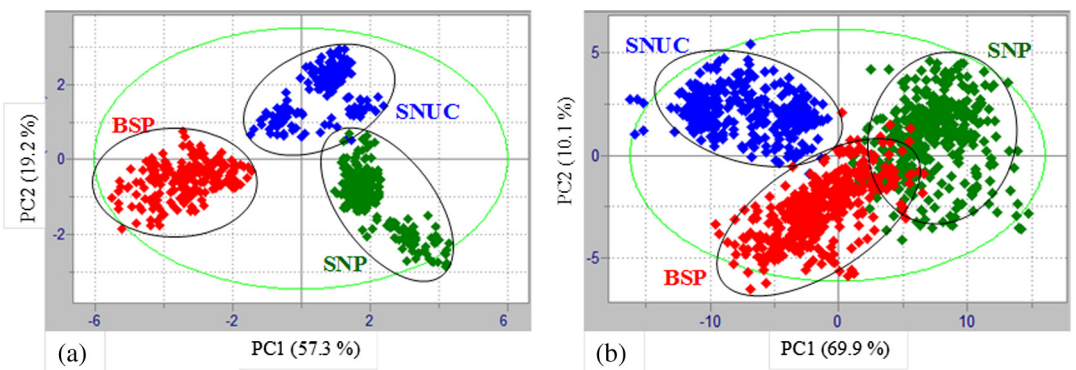

Fig. 4 PCA scores plots (PC1 versus PC2) of IR spectra corresponding to: (a) epithelia and (b) connectives found in SNP, BSP, and SNUC samples. The percentages in brackets represent the spectral variability of each component.

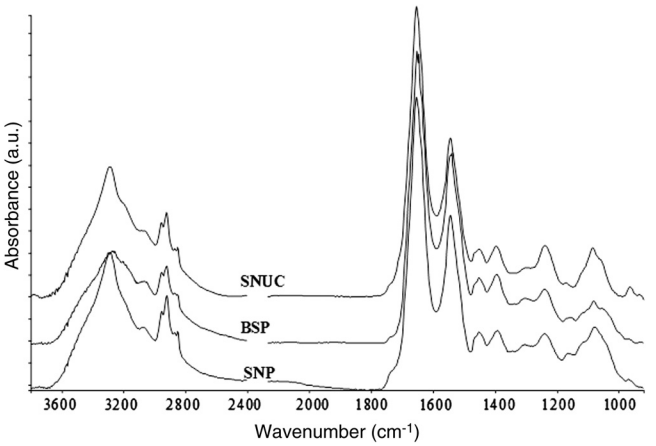

Fig. 5 Absorbance average spectra of the various epithelia found in SNP, BSP, and SNUC sections. The spectra were vector normalized and two-points baseline linear fitted in the range 3800 to 900 cm^{-1}. For reasons of clarity, BSP and SNUC spectra were shifted along the *y*-axis (absorbance was expressed in arbitrary units).

The IR region 3050 to 2800 cm^{-1}, usually referred to as the lipid component, includes the symmetric and asymmetric stretching modes of CH_2 and CH_3 alkyl groups and the stretching vibration of =CH moiety. In all average spectra of the epithelia, the following absorptions were detected: 3013 ± 2 (ν=CH), 2959 ± 1 ($\nu_{asym}CH_3$), 2924 ± 1 ($\nu_{asym}CH_2$), 2870 ± 1 ($\nu_{sym}CH_3$), and 2850 ± 1 ($\nu_{sym}CH_2$) cm^{-1}. The resulting band-area ratios were calculated: 3013/2959 (unsaturation level) and 2924/2959 (alkyl chains' length and saturation level) (Table 1). With respect to the respiratory epithelium, the transitional and tumoral ones showed lower values of the ratio 2924/2959, suggesting a decrease in CH_2 groups, which could correspond to shorter lipid alkyl chains in BSP and SNUC epithelia.[17,18] In all the samples, a very weak band at 3013 cm^{-1}, better detected in DII mode, was found, corresponding to =CH moieties. The trend of the band-area ratio 3013/2959 shows a higher degree of unsaturation in the tE.[18,19]

Amide I and II bands elucidate proteins secondary structures. In our case, the following absorption bands were found:

Table 1 Numerical variations of meaningful band-area ratios for the epithelia found in SNP, BSP, and SNUC lesions. Values indicate mean ± SD. Significant differences between experimental groups were determined as detailed in Sec. 2 and are indicated by asterisks: #*P* nonsignificant; **P* < 0.05; ***P* < 0.01; and ****P* < 0.001.

Band-area ratios	SNP	BSP	SNUC	Biochemical features	*P* values
3013/2959 (ν=CH/$\nu_{asym}CH_3$)	0.0063 ± 0.0005	0.0060 ± 0.0006	0.0104 ± 0.0008	Unsaturation level	SNP versus BSP$^{\#}$ BSP versus SNUC*** SNP versus SNUC***
2924/2959 ($\nu_{asym}CH_2/\nu_{asym}CH_3$)	1.89 ± 0.02	1.19 ± 0.03	1.32 ± 0.02	Saturation level	SNP versus BSP*** BSP versus SNUC$^{\#}$ SNP versus SNUC***
Helix/AI	0.53 ± 0.05	0.51 ± 0.08	0.60 ± 0.06	Proteins secondary structure	SNP versus BSP* BSP versus SNUC** SNP versus SNUC***
β/AI	0.29 ± 0.02	0.25 ± 0.04	0.21 ± 0.02		SNP versus BSP* BSP versus SNUC* SNP versus SNUC***
Random/AI	0.18 ± 0.02	0.24 ± 0.03	0.24 ± 0.01		SNP versus BSP*** BSP versus SNUC* SNP versus SNUC*
1745/AI (νC=O ester/AI)	0.0133 ± 0.001	0.0083 ± 0.0007	0.0103 ± 0.001	Lipid amount	SNP versus BSP*** BSP versus SNUC*** SNP versus SNUC***
1310/AI (keratin/AI)	0.0098 ± 0.001	0.0169 ± 0.002	0.0207 ± 0.002	Keratin amount	SNP versus BSP*** BSP versus SNUC$^{\#}$ SNP versus SNUC***
1120/1021 (RNA/DNA)	2.23 ± 0.2	1.81 ± 0.3	9.42 ± 0.1	Cellular proliferation	SNP versus BSP$^{\#}$ BSP versus SNUC*** SNP versus SNUC***
1050/1086 (glycogen/$\nu_{sym}PO_{2^-}$)	0.71 ± 0.08	0.40 ± 0.03	0.48 ± 0.02	Glycogen amount	SNP versus BSP** BSP versus SNUC*** SNP versus SNUC***
1154/1171 (νCOH/νCOP)	0.87 ± 0.05	0.71 ± 0.04	0.48 ± 0.04	Phosphorilative processes	SNP versus BSP* BSP versus SNUC** SNP versus SNUC**

1697 ± 2, 1680 ± 1, and 1621 ± 3 cm^{-1} (β structures); 1668 ± 1 and 1657 ± 1 cm^{-1} (helix components); 1639 ± 1 cm^{-1} (random coil structures); 1555 ± 1 cm^{-1} (helix and random coil structures); and 1538 ± 3 cm^{-1} (β structures). According to amide I, meaningful band-area ratios were calculated: helix/AI, β/AI, and random/AI, where AI is amide I total area (Table 1). In particular, a decrease in β-sheet components was found in the tE (SNUC), together with a small increase in helix and random coil structures.[20,21]

A weak band at 1745 cm^{-1} (usually attributed to the stretching vibration of ester carbonyls of triglycerides) was found in all epithelia but was weaker in BSP and SNUC samples (Fig. 5). By analyzing the trend of the band ratio 1745/AI, a higher consumption of lipids could be conceivable in the tumoral lesions.[17]

The increase in the band ratio 1310/AI, both in BSP and SNUC epithelia, confirms the presence of keratin and, as a consequence, the squamous nature of these two lesions (Table 1).[22]

The spectral region 1350 to 920 cm^{-1} includes the main vibrations of nucleic acid functional groups. In the tE (SNUC), an increase in the band-area ratio 1120/1021 (RNA/DNA), together with a decrease in 1050/1086 (glycogen/$\nu_{sym}PO_{2^-}$), was found, confirming the high degree of malignancy with a hypercellular proliferation and an enhanced consumption of glycogen.[11,23,24] In SNUC, the presence of phosphorilative processes was also pinpointed by the trend of the band-area ratio 1154/1171 (νCOH/νCOP) (Table 1).[25]

3.2 *Vibrational Analysis of Connective Tissues*

As mentioned above, some epithelial tumors may infiltrate and modify the neighboring connective tissue, inducing evident morphological and structural modifications in it.[12,16] To better highlight this aspect, absorbance average spectra of connective tissues in SNP, BSP, and SNUC samples were analyzed by the peak-fitting procedure in the spectral range 1480 to 920 cm^{-1}, in which the most significant bands attributable to collagen are present. The following trends were found (Fig. 6): (i) an increase in the band-area ratio 1397/1450 ($\nu_{sym}COO-/\delta CH_{2/3}$), suggesting more evident peroxidative processes in SNUC;[16,26] (ii) an increase in the band-area ratio 1082/1238, typical of tumoral tissues;[27,28] and (iii) a decrease in the side bands in the characteristic tricuspid shape of collagen (1281, 1238, and 1202 cm^{-1}).[29]

4 Conclusions

FTIRI might represent a valid complementary tool in clinical analysis and prognosis, especially when it is difficult to make an indubitable diagnosis by exploiting only conventional methodologies. In fact, it has been well ascertained that FTIRI could detect at a molecular level the biological modifications in pathological tissues, even before they can be discovered using routine diagnostic assays.

In this light, this contribution represents a starting point in the assessment of FTIRI to achieve an objective diagnosis of some recurring sinonasal lesions, such as SNPs, BSPs, and SNUCs. In particular, specific spectral features of the various epithelium layers and, to a further extent, of the neighboring connective tissues were defined to discriminate malignant lesions from benign and inflammatory ones.

The tE found in the undifferentiated sinonasal carcinoma shows, with respect to the respiratory one, the occurrence of peroxidative (3013/2959, ν=CH/$\nu_{asym}CH_3$) and phosphorilative (1154/1171, νCOH/νCOP) processes, a modified proteins secondary structure (with a decrease in β-sheets components and a small increase in helix and random coil structures), a major consumption of lipids (1745/AI, νC=O ester/AI) and glycogen (1050/1086, glycogen/$\nu_{sym}PO_{2^-}$), and a higher cellular proliferation (1120/1021, RNA/DNA). The squamous nature of this lesion is confirmed by the presence of keratin (1310/AI, keratin/AI) and also of a modified connective tissue. The trE of the Schneiderian papilloma, which shows some features similar to the tumoral one (a higher consumption of lipids and glycogen and the presence of keratin), is characterized by shorter alkyl chains (2924/2959, $\nu_{asym}CH_2/\nu_{asym}CH_3$) and unordered proteins (an increase in random coil structures).

The application of this spectroscopic method in common clinical practice demands a larger cohort of patients and for the extension of the study to an increasing number of oral pathologies. However, this paper once more highlights the full potential of FTIRI in medical diagnosis.

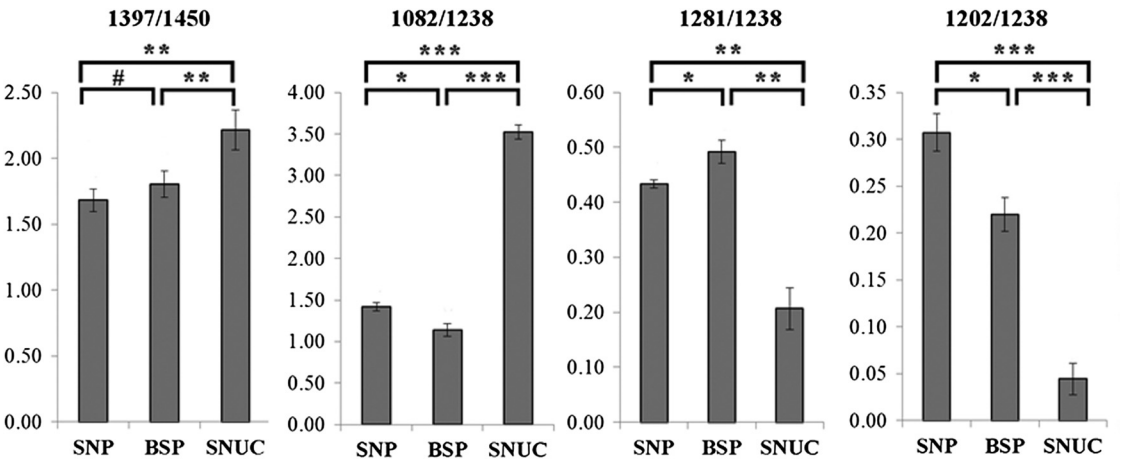

Fig. 6 Numerical variations of meaningful band-area ratios for the connective tissues found in SNP, BSP, and SNUC lesions: 1397/1450 ($\nu_{sym}COO-/\delta CH_{2/3}$), 1082/1238 ($\nu_{sym}PO_{2^-}/\nu_{asym}PO_{2^-}$), 1281/1238 (collagen/$\nu_{asym}PO_{2^-}$), and 1202/1238 (collagen/$\nu_{asym}PO_{2^-}$). Values indicate mean ± SD. Significant differences between experimental groups were determined as detailed in Sec. 2 and are indicated as follows: #P nonsignificant; *$P < 0.05$; **$P < 0.01$; and ***$P < 0.001$.

References

1. B. Perez-Ordenez, "Special tumours of the head and neck region," *Curr. Diagn. Pathol.* **9**, 366–383 (2003).
2. B. M. Wenig, *Atlas of Head and Neck Pathology*, 2nd ed., Saunders, Elsevier, Amsterdam, The Netherlands (2008).
3. J. B. Epstein et al., "Analysis of oral lesion biopsies identified and evaluated by visual examination, chemiluminescence and toluidine blue," *Oral Oncol.* **44**, 538–544 (2008).
4. R. K. Dukor, "Vibrational spectroscopy in the detection of cancer," in *Handbook of Vibrational Spectroscopy*, J. M. Chalmers and P. R. Griffiths, Eds., pp. 3335, John Wiley and Sons Ltd., Chichester, UK (2002).
5. N. S. Eikje, K. Aizawa, and Y. Ozaki, "Vibrational spectroscopy for molecular characterisation and diagnosis of benign, premalignant and malignant skin tumours," *Biotechnol. Ann. Rev.* **11**, 191–225 (2005).
6. A. Kallenbach-Thieltges et al., "Immunohistochemistry, histopathology and infrared spectral histopathology of colon cancer tissue sections," *J. Biophotonics* **6**, 88–100 (2013).
7. M. J. Baker et al., "FTIR-based spectroscopic analysis in the identification of clinically aggressive prostate cancer," *Br. J. Cancer* **99**, 1859–1866 (2008).
8. G. E. Menzies et al., "Fourier transform infrared for noninvasive optical diagnosis of oral, oropharyngeal, and laryngeal cancer," *Transl. Res.* **163**, 19–26 (2014).
9. K. Badizadegan et al., "Spectroscopic diagnosis and imaging of invisible pre-cancer," *Faraday Discuss.* **126**, 265–279 (2004).
10. G. Tosi et al., "FTIR microspectroscopy of melanocytic skin lesions: a preliminary study," *Analyst* **135**, 3213–3219 (2010).
11. S. Sabbatini et al., "Infrared microspectroscopy of oral squamous cell carcinoma: spectral signatures of cancer grading," *Vib. Spectrosc.* **68**, 196–203 (2013).
12. G. Tosi et al., "Microimaging FT-IR of head and neck tumors. V. Odontogenic cystic lesions," *Vib. Spectrosc.* **57**, 140–147 (2011)..
13. E. Giorgini et al., "FTIR microspectroscopic characterization of Spitz nevi," *Spectrochim. Acta Part A* **141**, 99–103 (2015).
14. A. S. Garcia et al., "Squamous cell carcinoma arising from inverted Schneiderian papilloma: a case report with oral involvement," *Case Rep. Otolaryngol.* **2014**, 478092 (2014).
15. C. Beleites and V. Sergo, "HyperSpec: a package to handle hyperspectral data sets in R," Rpackage version 0.98-20120224, *J. Stat. Software*, http://hyperspec.r-forge.r-project.org, in preparation.
16. C. Conti et al., "Microimaging FTIR of head and neck tumors. IV," *Microsc. Res. Tech.* **72**, 67–75 (2009).
17. J. G. Wu et al., "Distinguishing malignant from normal oral tissues using FTIR fiber-optic techniques," *Biopolymers* **62**, 185–192 (2001).
18. C. Petibois and G. Deleris, "Chemical mapping of tumor progression by FT-IR imaging: towards molecular histopathology," *Trends Biotechnol.* **24**, 455–462 (2006).
19. F. Severcan et al., "Rapid monitoring of diabetes-induced lipid peroxidation by Fourier transform infrared spectroscopy: evidence from rat liver microsomal membranes," *Anal. Biochem.* **339**, 36–40 (2005).
20. E. Giorgini et al., "FT-IR microscopic analysis on human dental pulp stem cells," *Vib. Spectrosc.* **57**, 30–34 (2011)..
21. W. Jeong and H. C. Shin, "Formation of an α-helix in human tumor necrosis factor-α by guanidine hydrochloride-induced unfolding," *Mol. Cells* **17**, 62–66 (2004).
22. C. Conti et al., "Microimaging FT-IR of oral cavity tumors. Part III: cells, inoculated tissues and human tissues," *J. Mol. Struct.* **834–836**, 86–94 (2007).
23. S. Argov et al., "Diagnostic potential of Fourier-transform infrared microspectroscopy and advanced computational methods in colon cancer patients," *J. Biomed. Opt.* **7**(2), 248–254 (2002).
24. J. Ramesh et al., "FTIR microscopic studies on normal, polyp, and malignant human colonic tissues," *Subsurface Sens. Tech. Appl.* **2**, 99–117 (2001).
25. M. J. Walsh et al., "Fourier transform infrared microspectroscopy identifies symmetric PO_{2^-} modifications as a marker of the putative stem cell region of human intestinal crypts," *Stem Cells* **26**, 108–118 (2008).
26. E. Giorgini et al., "Insights on diagnosis of oral cavity pathologies by infrared spectroscopy: a review," *J. Mol. Struct.* **1051**, 226–232 (2013).
27. C. Conti et al., "FT-IR microscopy imaging on oral cavity tumors, II," *J. Mol. Struct.* **744–747**, 187–193 (2005).
28. M. J. Tobin et al., "Infrared microscopy of epithelial cancer cells in whole tissues and in tissue culture, using synchrotron radiation," *Faraday Discuss.* **126**, 27–39 (2004).
29. K. Belbachir et al., "Collagen types analysis and differentiation by FTIR spectroscopy," *Anal. Bioanal. Chem.* **395**, 829–837 (2009).

Elisabetta Giorgini received her degree in chemistry from the University of Camerino (1987) and her PhD in chemical sciences from the University of Ancona (1993). She is the coauthor of 72 scientific papers and 70 contributions to international meetings. She is a researcher at the Polytechnic University of Marche. She is the director of the research unit of Ancona in the National Consortium CIRCSMB. She is engaged in vibrational studies of biological samples.

Simona Sabbatini received her degree in biological sciences from the Polytechnic University of Marche (2000) and her PhD in chemical sciences from the University of Ferrara. She is a researcher at the Polytechnic University of Marche, Ancona. She is coauthor of 30 scientific papers on peer-reviewed journals and 42 contributions to international meetings. She is focused on FT-IR imaging microspectroscopy of human cells, tissues, and biomaterials.

Carla Conti has been a spectroscopy technician at the Polytechnic University of Marche since 1980. She is part of the team for the emergency management, prevention, and protection against hazards at work. She is engaged in several scientific research programs on the application of imaging techniques. She is coauthor of 55 scientific papers, and she has attended several national and international meetings.

Corrado Rubini received his MD degree in medicine and surgery (1981) and his specialization degree in anatomic pathology (1985) from the University of Ancona. He is coauthor of 183 scientific papers and 11 contributions to international meetings. He is medical director, S.O.D. of anatomic pathology, "Ospedali Riuniti Umberto I", Ancona. He is engaged in the diagnosis and prognosis of preneoplastic and neoplastic lesions of oral mucous membrane.

Romina Rocchetti received her degree in biological sciences from the University of Urbino (1995) and her PhD in biomedical biotechnology from the Polytechnic University of Marche (2004). She is coauthor of 16 scientific papers, and she attended several national and international meetings. She has focused her research on the identification and characterization of cancer stem cells from oral squamous carcinoma cell lines.

Massimo Re received his MD degree in medicine and surgery from the University of Rome "La Sapienza" (1990) and his specialization degree in otorinolaringoiatry from the University of Pisa (1994). In 2000, he was a research/fellowship contributor at the Department of Otolaryngology, Mount Sinai Hospital, University of Toronto, Canada. He is coauthor of 75 scientific papers. He is medical director, S.O.D. of otolaryngology, "Ospedali Riuniti Umberto I", Ancona.

Lisa Vaccari received her MSc in chemistry (1999) and her PhD in pharmaceutical (2005) from Trieste University. From 1999 to 2006, she worked in the LILIT laboratory at Elettra—Sincrotrone Trieste. She is responsible for the life-science branchline of the infrared beamline at Elettra—Sincrotrone Trieste, SISSI. Her current research focuses on FTIR-microscopy of live cells under physiological conditions. She is coauthor of 50 scientific papers, and she attended numerous international meetings.

Elisa Mitri received her BS degree in chemistry and her PhD degree in nanotechnology from the University of Trieste in 2010 and 2014, respectively. Currently, she is a researcher at the SISSI Beamline of Elettra—Sincrotrone in Trieste. Her current research topic concerns the exploitation of infrared microspectroscopy in microfluidic devices as an analytical tool for *in vivo* investigation of biological systems.

Vito Librando received his degree in chemistry from the University of Catania. Currently, he is full professor of environmental chemistry at the University of Catania. His research deals with the environmental field, with particular attention to the characterization and reactivity of micropollutants. He is referee for several international journals. He is coauthor of 109 scientific papers and 125 contributions to international meetings.